Article

Optoelectronic and Charge Transport Properties at Organic#Organic Semiconductor Interfaces: Comparison between Polyfluorene-Based Polymer Blend and Copolymer

Ji-Seon Kim, Linus Lu, Paiboon Sreearunothai, Alex Seeley, Keng-Hoong Yim, Annamaria Petrozza, Craig E. Murphy, David Beljonne, Je#ro#me Cornil, and Richard H. Friend

J. Am. Chem. Soc., **2008**, 130 (39), 13120-13131 • DOI: 10.1021/ja803766j • Publication Date (Web): 04 September 2008

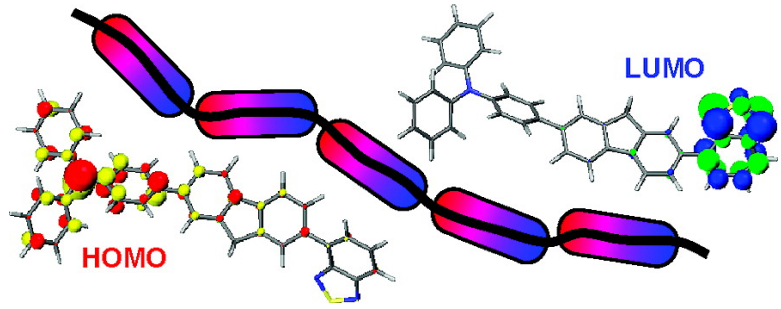

More About This Article

Additional resources and features associated with this article are available within the HTML version:

- Supporting Information
- Access to high resolution figures
- Links to articles and content related to this article
- Copyright permission to reproduce figures and/or text from this article

View the Full Text HTML

J|A|C|S
ARTICLES

Published on Web 09/04/2008

Optoelectronic and Charge Transport Properties at Organic−Organic Semiconductor Interfaces: Comparison between Polyfluorene-Based Polymer Blend and Copolymer

Ji-Seon Kim,*[,†,‡] Linus Lu,[†] Paiboon Sreearunothai,[†] Alex Seeley,[†] Keng-Hoong Yim,[†] Annamaria Petrozza,[†] Craig E. Murphy,[⊥,§] David Beljonne,[||] Jérôme Cornil,[||] and Richard H. Friend[†]

Cavendish Laboratory, University of Cambridge, J. J. Thomson Avenue, Cambridge CB3 0HE, U.K., Blackett Laboratory, Imperial College London, Prince Consort Road, London SW7 2AZ, U.K., Cambridge Display Technology Ltd., Cambourne Business Park, Cambridgeshire CB23 6DW, U.K., and Laboratory for Chemistry of Novel Materials, University of Mons-Hainaut, Place du Parc 20, B-7000 Mons, Belgium

Received May 20, 2008; E-mail: jkim1@imperial.ac.uk

Abstract: We report detailed studies of optoelectronic and charge transport properties at the organic−organic semiconductor interfaces formed between polymer chains (interchain) and within a polymer chain (intrachain). These interfaces are fabricated using poly(9,9-di-*n*-octylfluorene-*alt*-*N*-(4-butylphenyl)diphenylamine) (TFB [f8-tfb]) (electron-donor) and poly(9,9-di-*n*-octylfluorene-*alt*-benzothiadiazole) (F8BT [f8-bt]) (electron-acceptor) conjugated polymers, by blending them together or by covalently attaching them via a main polymer backbone (copolymer). For optoelectronic properties, when a bulky and twisted tfb molecule is incorporated into a rigid F8BT conjugated backbone, it disturbs the conjugation of F8BT polymer, leading to a blue-shift in the lowest absorption transition. However, by acting as an effective electron donor, it assists the formation of an intrachain singlet exciton that has a strong charge-transfer character, leading to a red-shifted and longer-lived emission than that of F8BT. An extremely efficient and fast energy transfer from tfb donor to bt acceptor is observed in the copolymer (<1 ps) compared to transfer from TFB to F8BT in the blend (tens of ps). This efficient energy transfer in the copolymer is found to be associated with its low fluorescence efficiency (40−45% vs 60−65% for blend) because of the migration of radiative singlet excitons to low-energy states such as triplet and exciplex states that are nonemissive or weakly emissive. The presence of molecular-scale tfb-f8-bt interfaces in the copolymer, however, does not hinder an efficient transport of charge carriers at high drive voltages. Instead, it provides a better balance of charge carriers inside the device, which leads to slower decay of the device efficiency and thus more stable light-emitting diodes with increasing voltage than the blend devices. These distinctive optoelectronic and charge transport properties observed at different organic−organic semiconductor interfaces will provide useful input for the design rules of conjugated polymers required for improved molecular electronics.

Introduction

Research efforts into organic semiconductors over the past decade have demonstrated the versatility of these materials in a wide range of applications.[1] Organic semiconductors combine the semiconductor properties traditionally associated with inorganic materials with the more desirable properties of plastics such as low cost, flexibility and ease of processing, and patterning. Moreover, the organic syntheses of these materials allow for great flexibility in the tuning of their electronic and optical properties.[1] By combining these properties, organic semiconductors such as conjugated polymers have been demonstrated as the active layer in light-emitting diodes (LEDs),[1,2] field-effect transistors (FETs),[3,4] and photovoltaic (PV) cells.[5,6] These conjugated polymers, on the other hand, provide a new way of looking at many of the broad fundamental scientific issues about using molecules for electronics, which are explored in many different materials systems down to the single-molecule scale.[7]

A great deal of the physics, which governs the behavior of molecules for electronics, occurs at the organic−organic semiconductor heterojunction. It determines the fate of excitons

[†] University of Cambridge.
[‡] Imperial College London.
[§] Cambridge Display Technology Ltd.
[||] University of Mons-Hainaut.
[⊥] Current address: National Physical Laboratory (NPL), Hampton Road, Teddington TW11 0LW, UK.

(1) Friend, R. H.; Gymer, R. W.; Holmes, A. B.; Burroughes, J. H.; Marks, R. N.; Taliani, C.; Bradley, D. D. C.; Dossantos, D. A.; Brédas, J. L.; Logdlund, M.; Salaneck, W. R. *Nature* **1999**, *397*, 121.
(2) Cao, Y.; Parker, I. D.; Yu, G.; Zhang, C.; Heeger, A. J. *Nature* **1999**, *397*, 414.
(3) Sirringhaus, H.; Tessler, N.; Friend, R. H. *Science* **1998**, *280*, 1741.
(4) Chua, L. L.; Chang, J.-F.; Zaumseil, J.; Ou, E. C. W.; Ho, P. K. H.; Sirringhaus, H.; Friend, R. H. *Nature* **2005**, *434*, 194.
(5) Halls, J. J. M.; Walsh, C. A.; Greenham, N. C.; Marseglia, E. A.; Friend, R. H.; Moratti, S. C.; Holmes, A. B. *Nature* **1995**, *376*, 498.
(6) Yu, G.; Gao, J.; Hummelen, J. C.; Wudl, F.; Heeger, A. J. *Science* **1995**, *270*, 1789.

 10.1021/ja803766j CCC: $40.75

to be either stabilized or destabilized at the interfaces. The former case produces efficient LEDs and the latter produces efficient PV cells.[8−10] For example, devices fabricated with poly(9,9-di-*n*-octylfluorene-*alt*-benzothiadiazole) (F8BT) blended with poly(9,9-di-*n*-octylfluorene-*alt*-*N*-(4-butylphenyl)diphenylamine) (TFB) work as efficient LEDs, which produce yellow-green emission with very low threshold voltages for light emission (<2 V) and efficiencies above 18 lm/W. In contrast, the devices fabricated with F8BT blended with poly(9,9-di-*n*-octylfluorene-*alt*-bis-*N*,*N*′-(4-butylphenyl)bis-*N*,*N*′-phenyl-1,4-phenylenediamine) (PFB) do not show improved LED performance but show high charge photogeneration working as efficient PV cells.[9,10]

In molecular semiconductors, these heterojunctions are generally fabricated as multiple-layer structures by successive vacuum sublimation steps.[11] However, in solution-processed conjugated polymers it is possible to make 'distributed heterojunctions' by the demixing of two dissimilar polymers spin-coated from a common solution with a range of processability and tunability.[12−14] When polymer films are formed by spin-coating and subsequent solvent removal, the polymers phase-separate, as is generally the case for noninteracting polymers,[15−17] and the interpenetrating network of the two polymers can provide a distributed interchain heterojunction structure. The organic−organic heterojunctions can be formed not only between two dissimilar polymers but also within a polymer chain (intrachain heterojunction) when two or more dissimilar molecular units, i.e. one acting as an electron-donor and the other as an electron-acceptor, are covalently attached together to form a main conjugated polymer backbone. Different electronic structures such as HOMO (the highest occupied molecular orbital) and LUMO (the lowest unoccupied molecular orbital) levels and an optical band gap of the materials, and different electronic processes involving optical and electrical excitations and charge transport, are expected across these interchain and intrachain heterojunctions. Although π-conjugated molecules and polymers with such intrachain donor−acceptor architectures have been previously synthesized in phenylquinoline-biphenothiazine,[18] carbazole-quinoline,[19] and poly(*p*-phenylenevinylene) derivatives containing aromatic triazole and oxadiazole systems,[20] there has been very little work performed on donor−acceptor heterojunctions fabricated with poly(fluorene)-based conjugated polymers that are currently of great interest for electronics applications.[21−27]

In this report, we present detailed studies on optoelectronic and charge transport properties at conjugated polymer−polymer heterojunctions fabricated with polyfluorene-based polymers. We use TFB (electron-donor and hole-transporter) and F8BT (electron-acceptor and electron-transporter) polymers to fabricate interchain and intrachain heterojunctions, by blending them together (blend) or by covalently attaching them to a main conjugated polymer backbone (copolymer). We study the electronic structures and electronic processes across these F8BT:TFB heterojunctions. The optical properties are examined in terms of absorption, steady state and transient photoluminescence, and photoinduced absorption of triplet excitons. Charge transport and recombination properties are studied in various device structures such as single-carrier devices, LEDs, and photovoltaic cells. On the basis of these observations, together with quantum-chemical calculations of the electronic structure of the materials, we discuss the important roles of organic−organic heterojunctions formed between F8BT:TFB polymer blend and copolymer.

Experimental Section

Polymer Solutions and Thin Films. F8BT (M_n = 110 kg/mol) and TFB (M_n = 60 kg/mol) homopolymers and F8BT:TFB random copolymer (M_n = 40 kg/mol) that has both F8BT and TFB units incorporated into the main conjugated polymer backbone were used as received from CDT Ltd. without further purification. Their chemical structures are shown in Figure 1. The random copolymer (RC) was synthesized by a Suzuki coupling reaction. Both hole-transporting triarylamine (tfb) and electron-transporting benzothiadiazole (bt) units are covalently attached to a main conjugated backbone of fluorene (f8) to form a tfb-f8-bt unit that has a strong intrachain donor−acceptor character. Polymer solutions were prepared by dissolving each polymer in *o*-xylene to produce a concentration of ∼12 mg/mL. For the blend, the F8BT and TFB solutions were mixed at a ratio of 50:50 (by weight). A ∼80−100 nm thick polymer layer was then spin-coated from these solutions on the top of the oxygen-plasma-treated quartz substrates. For the measurements of dilute solutions, each polymer solution was diluted to have a concentration of $\sim 10^{-3}$ to 10^{-4} mg/mL.

Differential Scanning Calorimeter. A Perkin-Elmer Pyris 1 DSC[27] was used to determine the transition temperatures of the samples. The DSC experiments involved three stages; samples were first heated from 30 °C at a constant rate to 300 °C, then held at 300 °C for 2 min, and cooled back down to 30 °C at the same rate. The cycle was then repeated for a second scan.

Raman Spectroscopy. A Renishaw 2000 Raman Microscope was used to collect Raman spectra.[12] Samples were excited with a HeNe laser (633 nm) focused on the sample with a 100× microscope objective, and the scattered Raman signal was collected

(7) (a) Reed, M. A.; Tour, J. M. *Sci. Am.* **2000**, *282*, 86. (b) Reinerth, M. A. *Nanotechnology* **1998**, *9*, 246. (c) Reed, M. A.; Zhou, C.; Muller, C. J.; Burgin, T. P.; Tour, J. M. *Science* **1997**, *278*, 252. (d) Strano, M. S. *Science* **2003**, *301*, 1519.
(8) Halls, J. J. M.; Cornil, J.; dos Santos, D. A.; Silbey, R.; Hwang, D. H.; Holmes, A. B.; Brédas, J. L.; Friend, R. H. *Phys. Rev. B* **1999**, *60*, 5721.
(9) Morteani, A. C.; Dhoot, A. S.; Kim, J. S.; Silva, C.; Greenham, N. C.; Friend, R. H.; Murphy, C. E.; Moons, E.; Cina, S.; Burroughes, J. H. *Adv. Mater.* **2003**, *15*, 1708.
(10) Morteani, A. C.; Sreearunothai, P.; Herz, L. M.; Friend, R. H.; Silva, C. *Phys. Rev. Lett.* **2004**, *92*, 247402–1.
(11) Tang, C. W.; VanSlyke, S. A. *Appl. Phys. Lett.* **1987**, *51*, 913.
(12) Kim, J. S.; Ho, P. K. H.; Murphy, C. E.; Friend, R. H. *Macromolecules* **2004**, *37*, 2861.
(13) Arias, A. C.; Mackenzie, J. D.; Stevenson, R.; Halls, J. J. M.; Inbasekran, M.; Woo, E. P.; Richards, D.; Friend, R. H. *Macromolecules* **2001**, *34*, 6005.
(14) Corcoran, N.; Arias, A. C.; Kim, J. S.; Mackenzie, J. D.; Friend, R. H. *Appl. Phys. Lett.* **2003**, *82*, 299.
(15) Jones, R. A. L.; Richards R. W. *Polymers at surfaces and Interfaces*; Cambridge University Press: Cambridge, 1999.
(16) Boltau, M.; Walheim, S.; Mlynek, J.; Krausch, G.; Steiner, U. *Nature* **1998**, *391*, 877.
(17) Walheim, S.; Schaffer, E.; Mylnek, J.; Steiner, U. *Science* **1999**, *283*, 520.
(18) Lai, R. Y.; Kong, X.; Jenekhe, A.; Bard, A. J. *J. Am. Chem. Soc.* **2003**, *125*, 12631.
(19) Jenekhe, S. A.; Lu, L.; Alam, M. *Macromolecules* **2001**, *34*, 7315.
(20) Chen, S.-H.; Chen, Y. *Macromolecules* **2005**, *38*, 53.
(21) Neher, D. *Macromol. Rapid Commun.* **2001**, *22*, 1365.
(22) Scherf, U.; List, E. J. W. *Adv. Mater.* **2002**, *14*, 477.
(23) Redeker, M.; Bradley, D. D. C.; Inbasekaran, M.; Wu, W. W.; Woo, E. P. *Adv. Mater.* **1999**, *11*, 241.
(24) Campbell, A. J.; Bradley, D. D. C.; Antoniadis, H. *Appl. Phys. Lett.* **2001**, *79*, 2133–2135.
(25) Herguth, P.; Jiang, X.; Liu, M. S.; Jen, A. K.-Y. *Macromolecules* **2002**, *35*, 6094–6100.
(26) He, Y.; Gong, S.; Hattori, R.; Kanicki, J. *Appl. Phys. Lett.* **1999**, *74*, 2265.
(27) Donley, C. L.; Zaumseil, J.; Andreasen, J. W.; Nielsen, M. M.; Sirringhaus, H.; Friend, R. H.; Kim, J. S. *J. Am. Chem. Soc.* **2005**, *127*, 12890.

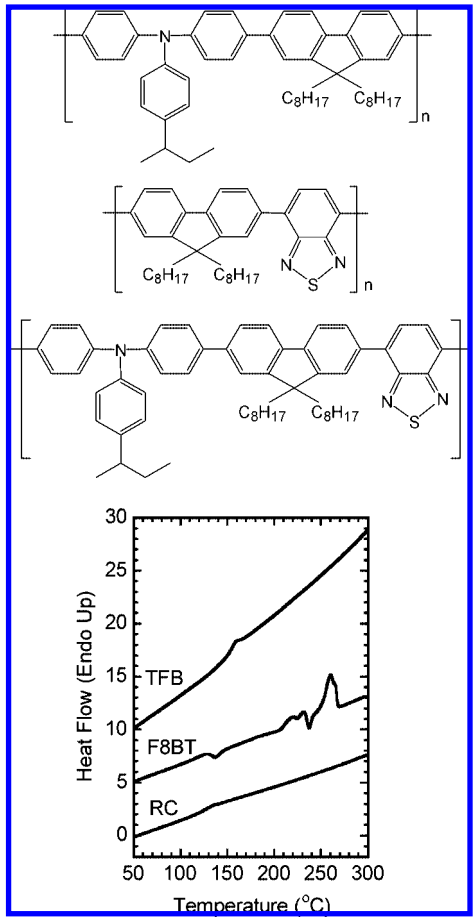

Figure 1. (Top) Chemical structures of TFB and F8BT polymers, and tfb-f8-bt unit that exists in RC. (Bottom) Differential scanning calorimetry (DSC) data for these materials. Only the second heating scans are shown.

through the same objective and detected by a CCD camera. A 20 s integration time was used, and the signal was summed over 10 scans in the extended scan mode. After irradiation, the samples were visually inspected through the microscope, but no signs of laser damage to the sample were observed.

Atomic Force Microscope. AFM (Digital Instruments Inc. NanoScope II) in the tapping mode was used to study the morphological features of the films. Optical microscope (Olympus BX 51) was used to take photoluminescence (PL) images of the films under blue excitation.

Absorption/ Emission Spectroscopy. Absorption spectra for solutions and thin films were acquired with a Hewlett-Packard 8453 diode array spectrometer. Both PL spectra and efficiencies were measured at room temperature in a nitrogen-purged integrating sphere with laser excitation at 457 nm or at 355/365 nm. PL efficiencies were calculated as described by de Mello and co-workers.[28]

Two different types of time-resolved spectroscopic techniques were used to study PL decay dynamics of polymer solutions and films in different time scales. They are a time-correlated single-photon counting (TCSPC) technique (a nanosecond time scale)[29] and an ultrafast up-conversion technique (a femtosecond time scale).[30] For TCSPC, PL decay curves were measured in the range of 500−700 nm with a step of 5 nm, using the second harmonic of a Ti:sapphire oscillator (3.05 eV) running at 87 Mhz as the pump source. The detection system was a microchannel plate photomultiplier tube coupled to spectrometer and TCSPC electronics. Films were measured in a front-excitation-front-detection configuration at room temperature under a dynamic vacuum of $<10^{-5}$ mbar to avoid photo-oxidation. Time-integrated PL spectra of these films were also measured (450−750 nm, integration: 1s/nm). For a femtosecond up-conversion technique, films were excited at room temperature under a vacuum of $\sim 10^{-6}$ mbar with the frequency-doubled output from a mode-locked Ti:sapphire laser at 3.1 eV with a temporal resolution of ~400 fs. PL originating from the samples were collected using dispersion-free optics and up-converted in a β-barium-borate crystal using the fundamental laser beam at 1.55 eV as a gate. Sum-frequency photons were dispersed in a monochromator and detected via single-photon counting.

Photoinduced absorption (PIA) spectroscopy was used to measure the yield of long-lived ($\approx \mu$s-ms) triplet excitons in the materials at low temperature (10−30 K).[31] While the sample was excited by a CW pump source (488 nm, 150 mW/cm^2) modulated mechanically by a chopper in a frequency at 224 Hz, the transmission (T) of the sample was monitored with a probe beam (white light source: 150 W halogen bulb) in an infrared range. A lock-in detection of the probe beam was used to measure small changes of the transmission (ΔT) in the sample. The transmitted light was detected by an amplified Si photodiode, whose signal output was measured by the lock-in amplifier with a reference signal provided by the chopper control unit.

Device Fabrications/Characterizations. LEDs and photovoltaic cells were fabricated by using oxygen-plasma-treated ITO anode[32] and Ca/Al cathode. A 60-nm-thick hole-injecting/transporting poly(styrene sulfonate)-doped poly(3,4-ethylene dioxythiophene) (PEDT:PSS) (Bayer) layer was first spin-coated from a water solution on the top of the ITO substrate and then baked at 150 °C for 15 min in an oven with N_2 flow. An 80−100-nm-thick active layer was then spin-coated on the top of the PEDT:PSS layer. Finally, the devices were completed by evaporating Ca (~20 nm) with Al (~200 nm) protecting layer at a base pressure better than 10^{-6} mbar. For single-carrier (hole-only or electron-only) devices, different combinations of electrodes were used. The low work function Ca electrode was replaced by a high work function NiCr electrode for hole-only devices and the ITO by a semitransparent Al (15 nm) electrode for electron-only devices. Devices were characterized in both DC and pulsed modes. For pulsed modes, devices were characterized under nanosecond-resolution pulsed EL, using a custom-built pulse generator, a photomultiplier tube, and a storage oscilloscope.[33]

Results and Discussion

Physical/Chemical Properties. a. DSC. The transition temperatures of TFB, F8BT, and random copolymer (RC) molecules were determined by DSC, and the second heating scans are shown in Figure 1. F8BT shows a first transition near 135 °C, which has been previously assigned to the transition from glassy to rubbery state with a certain degree of recrystallization due to the exothermic nature of the shift.[27,34] Continued heating of F8BT leads to a second exothermic transition (crystallization) at around 235 °C and a final endothermic transition due to melting (T_m) into a liquid crystalline phase at 260 °C.

TFB and RC exhibit an onset of the glass transition (T_g) near 150 and 130 °C, respectively. However, neither crystallization

(28) deMello, J. C.; Wittmann, H. F.; Friend, R. H. *Adv. Mater.* **1997**, *9*, 230.
(29) Osaheni, J. A.; Jenekhe, S. A.; Perlstein, J. *J. Phys. Chem.* **1994**, *98*, 12727.
(30) Herz, L. M.; Phillips, R. T. *Phys. Rev. B* **2000**, *61*, 13691.
(31) Ginger, D. S.; Greenham, N. C. *Phys. Rev. B* **1999**, *59*, 10622.
(32) Kim, J. S.; Granström, M.; Friend, R. H.; Johansson, N.; Salaneck, W. R.; Daik, R.; Feast, W. J.; Cacialli, F. *J. Appl. Phys.* **1998**, *84*, 6859.
(33) Seeley, A. J. A. B.; Friend, R. H.; Kim, J. S.; Burroughes, J. H. *J. Appl. Phys.* **2004**, *96*, 7643.
(34) Banach, M. J.; Friend, R. H.; Sirringhaus, H. *Macromolecules* **2003**, *36*, 2838.

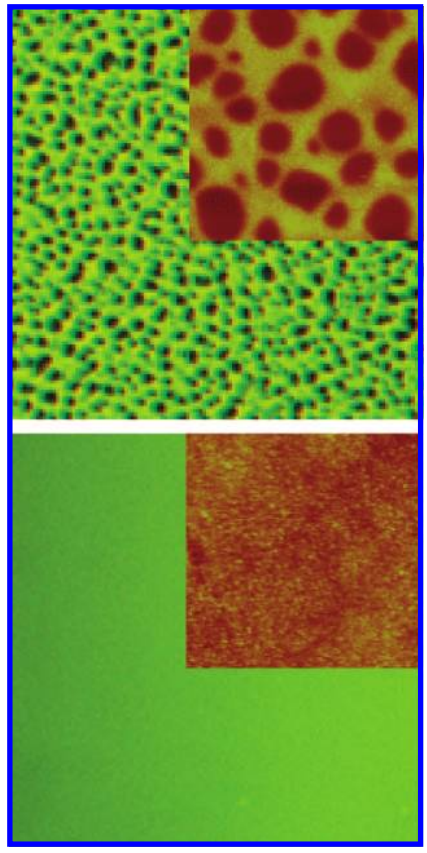

Figure 2. PL images (30 μm × 30 μm) of ∼100 nm thick F8B:TFB blend (50:50) (top) and RC (bottom) films. Inset: AFM images (5 μm × 5 μm) with 100 and 20 nm height scales for blend and RC films, respectively (bright: high region; dark: low region). On the basis of the PL of the blend film, it is concluded that the high ridges are F8BT matrix phase (bright regions in PL image) and the thin regions are TFB-rich enclosed phase (dark regions in PL image).

nor melting transitions are observed in these polymers, indicating a highly amorphous nature of these materials. We notice that the F8BT molecule loses its liquid crystalline character when copolymerized with a highly amorphous tfb molecule.

b. AFM and PL Microscopy. Figure 2 shows the optical images of PL under blue excitation and the tapping mode AFM images of the F8BT:TFB blend and RC thin films. For the blend film, there is a high matrix phase with a micrometer-length scale lower enclosed phase and the height difference being ∼25−30 nm. It should be noted that the lateral size of the features is much larger than the average film thickness (0.1 μm) and that there are relatively large variations in the height of the film surface (10 s nm). These characteristic surface feature sizes are formed to be not only composition dependent (polymer and solvent composition) but also processing dependent (temperature, postbake, etc.).[12−14] The distribution of phases seen in AFM data is quantitatively examined using the Bearing function. The depth distribution of the AFM scans is bimodal, indicating the presence of two main phases, the higher and the lower phases. For the RC film, the AFM image exhibits a very small rms roughness (1.5−2.0 nm) with no obvious surface structures.

The PL microscopy that allows identification of the F8BT under blue-excitation (excitation with blue light results in green luminescence from only F8BT) has confirmed that the higher-lying phases in the blend film are F8BT (or F8BT-rich) and lower-lying phases are TFB (or TFB-rich). On the other hand, the RC film shows a uniform green emission through the whole

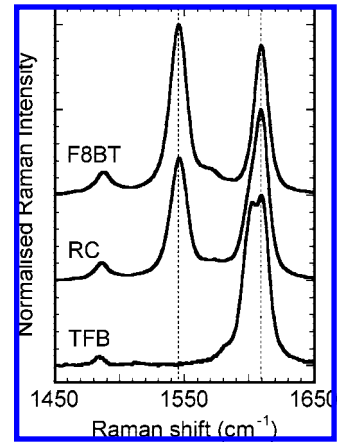

Figure 3. Normalized Raman spectra (633 nm excitation) of ∼100-nm-thick F8BT, RC, and TFB thin films on quartz substrates.

surface of the film with no observable domains, confirming the absence of phase-separated domains at the micron scale.

c. Raman Spectroscopy. In order to determine quantitatively the composition of the materials in different domains of the F8BT:TFB blend and RC thin films, we used Raman microscopy.[12,35−37] Figure 3 shows the normalized Raman spectra of ∼100-nm-thick neat F8BT, TFB, and RC films in the range of 1450−1650 cm^{-1}. The Raman spectrum of F8BT shows two strong Raman peaks at 1609 cm^{-1} (fluorene ring-stretch) and 1546 cm^{-1} (benzothiadiazole ring-stretch), and the Raman spectrum of TFB shows two strong but partially resolved Raman peaks at 1609 cm^{-1} (fluorene ring-stretch) and 1602 cm^{-1} (phenylene ring-stretch). The Raman spectrum of RC exhibits the Raman peaks originated from both F8BT and TFB homopolymers without any measurable shifts and broadening of the peaks. By taking into account the Raman scattering cross-section of two homopolymers,[12] we quantitatively assay the local composition of the RC at the micron scale. We find ∼45 ± 5% of F8BT and ∼55 ± 5% of TFB in this RC. A cross-mapping (40 μm × 40 μm) of the RC film by Raman microscopy shows less than 5% variation of the peak intensities at 1546 cm^{-1} (bt) and 1602 cm^{-1} (tfb), indicating a highly uniform and homogeneous distribution of different chemical compositions in the RC film.

The Raman spectra of F8BT:TFB blend films taken at two different phases, low and dark enclosed domains (TFB or TFB-rich) and high and bright matrix phases (F8BT or F8BT-rich), were previously investigated.[12] We found that each domain is not pure at the (sub)micron-length scale within each phase that appears pure to AFM and optical PL images. The TFB-rich domain has 20−25% F8BT and the F8BT-rich domain has 30−35% TFB.

Optoelectronic Properties. a. Absorption. The absorption spectra of the blend and RC dilute solutions (6 × 10^{-3} mg/mL) are in general linear combinations of that of each homopolymer, F8BT and TFB (Figure 4a). The lowest absorption band appears at ∼457 nm for F8BT and F8BT in the blend solution. This band, however, is slightly blue-shifted (∼13 nm) in RC solution. Such a blue-shift in the first absorption band in

(35) Kim, J. S.; Ho, P. K. H.; Murphy, C. E.; Baynes, N.; Friend, R. H. *Adv. Mater.* **2002**, *14*, 206–209.
(36) Kim, J. S.; Ho, P. K. H.; Murphy, C. E.; Seeley, A. J. A. B.; Grizzi, I.; Burroughes, J. H.; Friend, R. H. *Chem. Phys. Lett.* **2004**, *386*, 2.
(37) Tian, B.; Zerbi, G.; Schenk, R.; Müllen, K. *J. Chem. Phys.* **1991**, *95*, 3191.

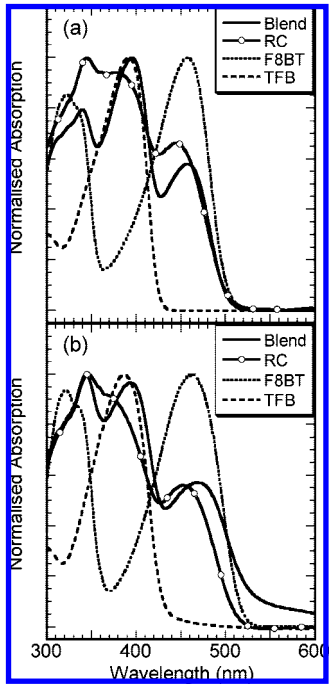

Figure 4. UV−visible absorption spectra of (a) solutions (6×10^{-3} mg/mL) and (b) thin films. A broadening of the absorption peaks upon film formation has been observed. The higher background at longer wavelengths for the blend film in (b) is due to an increase in scattering because of the high surface roughness of this film.

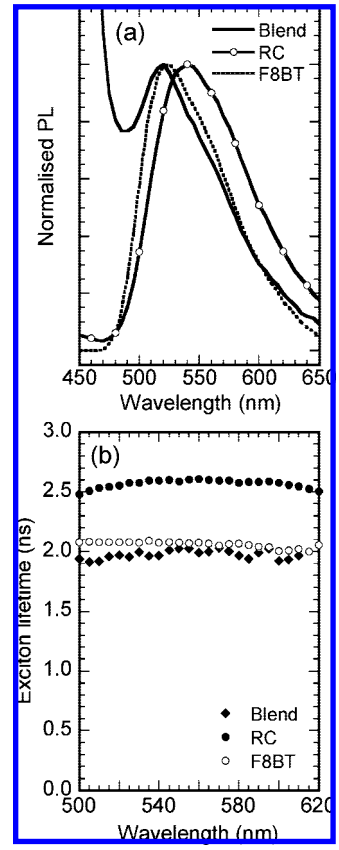

Figure 5. (a) Time-integrated PL spectra of blend, RC, and F8BT dilute solutions (6×10^{-4} mg/mL) and (b) the exciton lifetime as a function of emitted photon energy. PL decay curves were fitted with a monoexponential function to calculate the exciton lifetime values. The fitting error (χ^2) was typically <1.5, indicating that the fitted curves closely reproduce the experimental PL decay curves.

the RC can be understood by considering the presence of significantly twisted and bulky tfb units in the conjugated backbone that reduces the effective conjugation length of the F8BT polymer.

Compared to dilute solutions, the absorption spectra of most thin films show a red-shift of ∼5−7 nm in the lowest absorption band with a broadening of this band toward longer wavelengths (Figure 4b). A more planar conjugated polymer backbone or the polarizability effect[19,38] imposed upon thin film formation may be responsible for such changes. A more significant broadening together with higher scattering background is observed in the blend film due to a significant increase in the surface roughness of this film (25−30 nm).

The absorption spectra of blend and RC thin films are also in general linear combinations of that of each homopolymer, indicating no ground-state charge transfer occurring at the polymer−polymer interfaces formed during film formation in these materials. The absence of ground-state doping in these films was confirmed by photothermal deflection spectroscopy (PDS), a widely employed technique for investigation of subgap absorption in polymer films.[39] The lowest absorption band of the F8BT film is still blue-shifted (∼10 nm) in the RC film.

For neat TFB polymer, the lowest absorption band appears at ∼390 nm in the dilute solution and does not shift or broaden toward longer wavelengths on the thin film formation. Instead, the main peak position shifts slightly toward shorter wavelengths (<5 nm) with a very small broadening of the peak width. This indicates no planarization of the TFB chains gained going from a dilute solution to a solid state thin film. We attribute this effect to the more disordered morphology of TFB chains, resulting from conformational fluctuations of the highly twisted and bulky tfb units in the polymer backbone.[40]

b. Photoluminescence. Time-integrated PL spectra of dilute solutions (6×10^{-4} mg/mL) are shown in Figure 5a. The PL spectrum of F8BT solution exhibits the main emission peak at ∼520 nm with a shoulder peaking at ∼550 nm. For the blend solution, the PL spectrum is a linear combination of both F8BT and TFB emission, with much stronger TFB emission (<450 nm) due to its higher absorption coefficient under 3.05 eV excitation used and the relatively inefficient TFB-F8BT energy transfer. For the RC solution, the main F8BT emission peak is significantly red-shifted compared to that of neat F8BT, showing a peak at ∼540 nm with a strongly enhanced emission at longer wavelengths. A very small amount of TFB emission is observed in this RC, although ∼50% of TFB is incorporated into the polymer backbone of this material. This suggests an efficient intrachain energy transfer from tfb donor to bt acceptor in this RC chain.

The PL decay curves were measured at each emission wavelength of the materials (450−650 nm, 5 nm step) in dilute solutions and fitted with a monoexponential function to calculate the exciton lifetime.[29,41] The fitting error (χ^2) was typically <1.5, indicating that the fitted curves closely reproduce the experimental PL decay curves. The exciton lifetime for all the

(38) Gierschner, J.; Cornil, J.; Egelhaaf, H.-J. *Adv. Mater.* **2007**, *19*, 173.
(39) Ho, P. K. H.; Thomas, D. S.; Friend, R. H.; Tessler, N. *Science* **1999**, *285*, 233.
(40) Sancho-Garcia, J. C.; Foden, C. L.; Grizzi, I.; Greczynski, G.; deJong, M. P.; Salaneck, W. R.; Bredas, J. L.; Cornil, J. *J. Phys. Chem. B* **2004**, *108*, 5594.

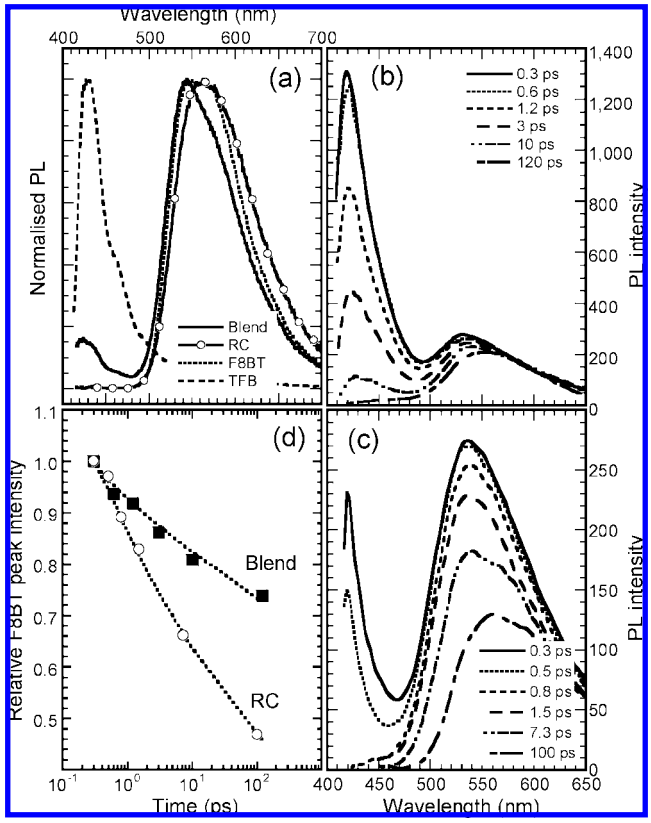

Figure 6. (a) Time-integrated PL spectra of blend, RC, F8BT, and TFB films (∼100 nm) at 3.05 eV excitation at room temperature under a vacuum of $<10^{-5}$ mbar. The time-resolved PL spectra of (b) blend and (c) RC films using a femtosecond up-conversion spectroscopy, and (d) the relative F8BT peak intensity as a function of decay time for blend and RC films, in which the F8BT peak intensity taken at 0.3 ps after laser excitation was normalized to be 1.0.

materials in dilute solutions is almost constant over a whole range of emitted photon energies (Figure 5b). The neat F8BT and F8BT in blend solution show an exciton lifetime of ∼2.0−2.1 ns. This exciton lifetime, however, increases up to ∼2.6 ns in the RC solution, which, together with a distinctive red-shift in the emission spectrum, points to a different nature of the emissive state in the RC.

For thin films, a 20−25 nm red-shift is observed in the PL spectra compared to their PL spectra of dilute solutions. For the neat F8BT film, the PL spectrum exhibits at least two main distinctive emission states at 545 and 570 nm (Figure 6a). These two states were previously determined to be separate emissive states, and the relative intensity of these states depends on the number of sites that are formed during film preparation, for example, as a function of the film thickness[41] and upon annealing.[27] Furthermore, the low energy state was found to be more strongly related to an order between F8BT molecules and thus suffer more severe quenching in a direct contact with quenching interfaces such as PEDT:PSS.[42] This low-energy emissive state of F8BT becomes more intense in the film compared to its dilute solution (Figure 6a vs Figure 5a), confirming that this state is more strongly coupled to the order between the F8BT molecules achieved during the film formation.

For the blend film, the PL spectrum is still dominated by the high energy component, similar to that observed in the F8BT dilute solution. This implies that the order between F8BT molecules obtained in neat polymer film is now largely disturbed by a disorder brought by amorphous TFB molecules. A very small amount of TFB emission at short wavelengths is observed in this blend film due to an efficient interchain energy transfer from TFB to F8BT in the solid state. This TFB emission totally disappears in the RC film, indicating much more efficient energy transfer occurring in this RC than in the blend.

c. Transient Photoluminescence. Such efficient and fast energy transfer processes occurring in these films were monitored by using a femtosecond up-conversion spectroscopy.[30] The transient PL spectra taken at the time scale of 0.3−120 ps after excitation are shown in Figure 6b and 6c for the blend and RC films, respectively. At 0.3 ps after excitation, TFB emits more strongly than F8BT in the blend film because of its higher absorption at the excitation energy used (3.12 eV). This strong TFB emission at 420 nm decays within ∼10 ps, transferring its energy to the F8BT. In contrast, in the RC film, TFB emission is already strongly reduced at 0.3 ps just after excitation, leading to a relatively low TFB emission compared to the F8BT emission. TFB emission then decays away quickly within 1 ps, which is 1 order of magnitude faster than the decay of TFB in the blend. This time-resolved PL of RC, together with its steady-state PL data showing a very small amount of TFB emission in the dilute solution (Figure 5a) and the total absence of the TFB emission in the film (Figure 6a), clearly demonstrate much faster and more efficient energy transfer from TFB to F8BT in the RC compared to that in the blend. We attribute this effect to the presence of molecular-scale intrachain and interchain TFB:F8BT interfaces in the RC.

We notice, however, that such efficient and fast energy transfer from TFB to F8BT occurring in the blend, and more strongly in the RC, does not increase the emission from F8BT. The relative peak intensity of F8BT emission in the blend and RC films is shown as a function of its decay time (Figure 6d). Within 100 ps, the intensity of F8BT emission decreases by more than 25% and 50% for the blend and RC films, respectively. A significant shift of the peak position toward longer wavelengths is also observed for both films (15−20 nm for F8BT and 25−30 nm for RC). Such decreases in the peak intensity of F8BT singlet excitons, with a red-shift of the emission peak, is strongly related to the formation of low-energy, long-lived, and weakly/nonemissive species such as separated charges, exciplexes,[10,43] and triplets[44] present in these films under photoexcitation, as shown below. These changes in the PL spectra are also correlated with the changes in PL quantum yield. The steady-state PL quantum yield was measured to be 0.7−0.8 for the neat F8BT film and decreased to 0.6−0.65 for the blend film and further to 0.4−0.45 for the RC film.

On a nanosecond time scale, both blend and RC films show the formation of red-shifted exciplex states. These are neutral excited states with a significant charge-transfer character and much longer-lived than singlet excitons (Figure 7).[9,10] The formation of these exciplexes will provide a possible loss mechanism in the quantum yield of radiative F8BT excitons and also be responsible for a significant shift of F8BT excitons

(41) Kim, J. S.; Grizzi, I.; Burroughes, J. H.; Friend, R. H. *Appl. Phy. Lett* **2005**, *87*, 023506.
(42) Yim, K. H.; Friend, R. H.; Kim, J. S. *J. Chem. Phys.* **2006**, *124*, 184706.
(43) Berggren, M.; Gustafsson, G.; Inganas, O.; Andersson, M. R.; Hjertberg, T.; Wennerstrom, O. *J. Appl. Phys.* **1994**, *76*, 7530.
(44) Ford, T. A.; Avilov, I.; Beljonne, D.; Greenham, N. C. *Phys. Rev. B* **2005**, *71*, 125212.

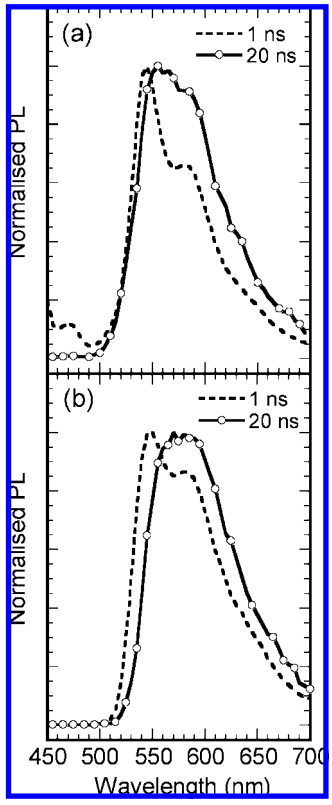

Figure 7. Time-resolved PL spectra of (a) blend and (b) RC films (3.05 eV excitation at 10 K under a vacuum of $<10^{-5}$ mbar).

toward longer wavelengths observed in ultrafast femtosecond transient PL spectra (Figure 6b and 6c).

d. Photoinduced Absorption. Recent work has shown that the yield of triplet excitons is enhanced in the polyfluoene-based blend systems as compared with constituent homopolymers because of an increased intersystem crossing (ISC) from singlet state to triplet state, mediated by the charge-separated state formed at the interchain polymer−polymer heterojunctions in the blends.[44] The formation of triplet excitons will provide an additional loss mechanism in the quantum yield of radiative excitons, since the triplet excitons have no dipole-allowed transition to the ground state and hence decay nonradiatively. A decrease in the PL quantum yield observed in the blend, and more strongly in the RC, can thus also be a result of a significant amount of triplet excitons formed in these materials under photoexcitation.

The yield of triplet excitons in these materials was measured by a photoinduced absorption (PIA) technique (excitation: 488 nm, 150 mW/cm^2).[31] Figure 8 shows the PIA spectra for films of neat F8BT, F8BT:TFB blend, and RC measured at 10−30 K. The optical density of these films was kept constant (∼0.8) at a wavelength corresponding to the first absorption peak of F8BT molecule. In this way, the magnitude of induced triplet absorption can be directly compared among these different samples without any difficulties induced by different amount of initial absorption by F8BT chromophores under photoexcitation.

All the films show a broad absorption feature peaking at around 1.45−1.53 eV, which is induced by the transition of triplet excitons to a higher-lying triplet state ($T_1 \rightarrow T_n$). The strength of this induced absorption at the triplet peak is very low ($\sim 0.36 \times 10^{-3}$) for the neat F8BT film but increases by ∼50% for the blend and significantly up to 7.5 times for the

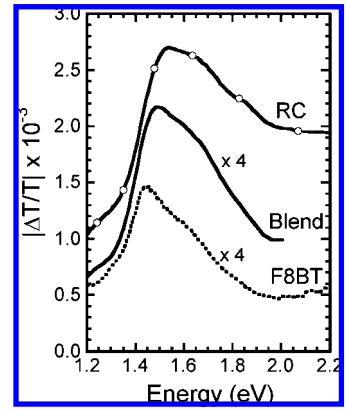

Figure 8. Photoinduced absorption spectra of RC, blend, and F8BT films taken under 150 mW/cm^2, 488 nm laser excitation at low temperature (10−35 K). The optical density of all films was kept constant (∼0.8) at the first peak of each absorption spectrum.

RC. The intensity- and frequency-dependent PIA studies show that the lifetime of triplet exctions in the RC is only two times longer than that of F8BT (∼0.5 ms vs ∼0.26 ms).

Assuming that the excitation is absorbed throughout the whole film, a relative change in transmission (and thus absorption) of photoinduced triplet excitons measured by PIA spectroscopy is governed by:

$$\left|\frac{\Delta T}{T}\right| = n\sigma d \qquad (1)$$

where n is the population of triplet excitons in the T_1 state, σ is the $T_1 \rightarrow T_n$ triplet absorption cross-section, and d is the thickness of the film. Based on a constant optical density for all samples producing a constant film thickness at an excitation wavelength and a small triplet absorption cross-section (σ) calculated for F8BT ($\sim 2 \times 10^{-16}$ cm^2),[44] the significant increase in the induced triplet absorption in RC can be attributed to an increase either in the population or in the lifetime of triplet T_1 excitons.

Since the lifetime of triplet excitons in the RC does not increase significantly compared to F8BT triplet excitons, we attribute such a dramatic increase in the yield of induced triplet absorption in the RC to an enhanced ISC process mediated by the intrachain charge-separated state. This leads to a strong quenching of singlet excitons and thus reduces the PL quantum yield of radiative singlet excitons. In addition to the charge-separated state formed between two dissimilar polymer chains as in the blend, a charge-separated state formed intramolecularly by the copresence of tfb donor and bt acceptor units in the RC may be responsible for such an effective ISC process and the resulting much higher triplet population in this material.

Device Characterizations. a. Single-Carrier Devices. The charge transport properties of these materials were investigated using single-carrier (hole- and electron-only) devices (Figure 9). For homopolymers, TFB exhibits about 2 orders of magnitude higher hole current than the electron current, and F8BT shows almost 3 orders of magnitude higher electron current than the hole current (not shown). The TFB hole-only device shows a sharp turn-on (threshold of 100 μA/cm^2) at 1.4 V, indicating a contact-limited injection for the holes, followed by a gradual increase in current. In contrast, the electron current for the F8BT device increases significantly as soon as the voltage is applied to the device with no distinguishable turn-on in current, indicating an ohmic contact for electron injection. Such different

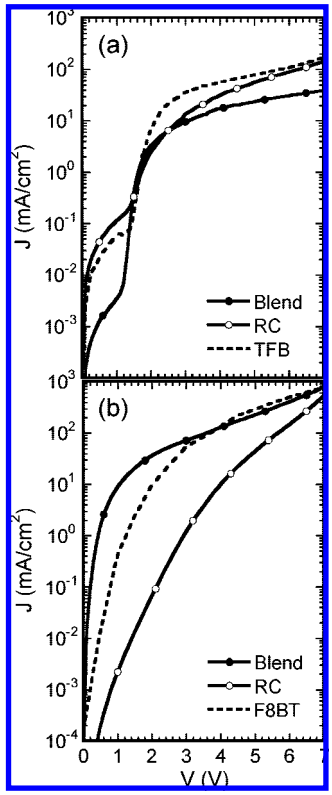

Figure 9. Current−voltage (J-V) characteristics of (a) hole-only and (b) electron-only devices.

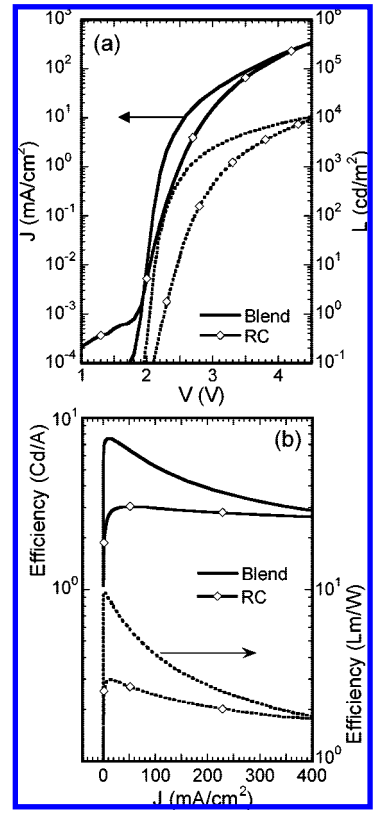

Figure 10. (a) Current−luminance-voltage (J-L-V) characteristics and (b) EL efficiencies (Cd/A and lm/W) as a function of diode current (J) for TFB:F8BT blend and RC LEDs.

characteristics for hole and electron currents in these homopolymers are expected from their different chemical and electronic properties; TFB has a relatively small ionization potential (∼5.33 eV) and a high hole mobility (∼10^{-3}-10^{-4} cm^2/Vs) suitable for efficient hole transport.[12,23,24] On the other hand, F8BT has a relatively large electron affinity (∼2.95 eV) with a high electron mobility (∼4 × 10^{-3} cm^2/Vs) suitable for efficient electron transport.[25−28]

Compared to these homopolymer devices (TFB hole-only and F8BT electron-only devices), the blend devices show a 70−80% decrease in hole current after turn-on with a large reduction in leakage current. This reduced hole current in the blend device may result from the lack of continuous transport pathways for holes in the blend film which shows distinctive micrometer-length scale enclosed TFB-rich domains (Figure 2a). On the other hand, the electron current increases much more steeply at <3 V than F8BT device but no significant changes at >3 V. This leads to more than 1 order of magnitude different hole and electron currents at high drive voltages in the blend devices.

For the RC devices, the hole current shows a similar reduction to the blend device just after turn-on but increases continuously to the same magnitude as the TFB device with increasing voltage (∼140 mA/cm^2 for RC and ∼170 mA/cm^2 for TFB at 7 V). The electron current exhibits a much slower rise at <4 V, leading to a large reduction in electron current at low drive voltages. It, however, increases steeply to the comparable values to the F8BT device at high drive voltages (∼550 mA/cm^2 for RC and ∼750 mA/cm^2 for F8BT at 7 V). These results indicate that the presence of molecular-scale tfb-f8-bt interfaces in the copolymer does not strongly hinder an efficient transport of charge carriers, in particular at high drive voltages. Instead, it may provide a better balance between the two charge carriers transported through the bulk of the film than that of the blend device. These balanced electron and hole currents in the RC plays an important role in determining the performance of double-carrier devices such as LEDs, as described below.

b. Light-Emitting Diodes. Work to examine the performance of LEDs with the blend and RC active layer has been performed (Figure 10). Both blend and RC LEDs exhibit well-behaved device characteristics, showing a turn-on in current (threshold of 0.2−0.3 μA/cm^2) at 1.6−1.8 V and luminance (threshold of 0.1 cd/m^2) at 2.0−2.2 V. The total current increases very steeply just after turn-on for the blend device but less steeply for the RC device, which leads to the higher total current in the blend device (<4 V). This higher total current that is originated from the higher electron current in the blend produces more than 1 order of magnitude higher luminance in the blend device than the RC device. The total current, however, becomes comparable for both devices as the voltage increases (>4 V), which yields the same magnitude of luminance (10 000 cd/m^2 at 4.5 V).

Because of their different charge transport and luminescence properties, the blend and RC LEDs yield significantly different characteristics of electroluminescence (EL) efficiencies as a function of voltage (or current). The blend LED shows high initial EL efficiencies (8 Cd/A, 10 lm/W) just after turn-on; however, these high efficiencies decay very fast as the device current increases (3 Cd/A, 2 lm/W at 400 mA/cm^2) (Figure 10b). In contrast, the RC LED exhibits lower initial EL efficiencies (3 Cd/A, 3 lm/W) after turn-on, but these initial efficiencies remain almost constant up to high current densities (only 10−30% drops compared to 60−80% drops in blend at 400 mA/cm^2). This slow decay of device efficiencies is attributed to a more balanced electron and hole transport through the RC, as described below. Such slower decay of device efficiencies

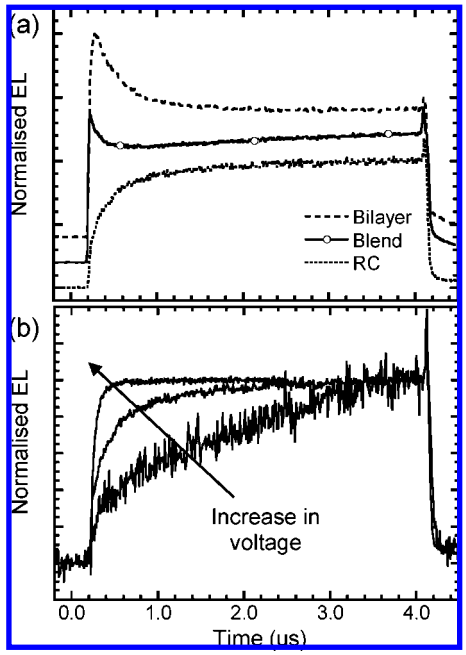

Figure 11. (a) Pulsed measurements of TFB:F8BT LEDs fabricated with bilayer (50 nm TFB/50 nm F8BT), polymer blend, and RC. A constant voltage pulse (5.5 V for the blend and 11−12 V for others) with the duration of 4 μs and 30 Hz repeat rate was used. (b) Pulsed measurements of the RC LED with an increase in the voltage from 6.5 V to 14.5 V.

at high voltages (or current) is an advantage for the fabrication of passive matrix displays in which much higher driving voltage (or current) is commonly used to produce the same level of brightness of the device as active matrix displays.

Charge balance inside the active layer has been studied by applying a pulse-mode electrical excitation to the device. The transient response of the devices under pulsed excitation yields important information related to charge injection and transport pathways,[45] in addition to its obvious use in high-brightness pulsed devices.[46] In our study, a constant voltage pulse (4 μs pulses with a repeat rate of 30 Hz) was sent to the devices and their transient EL characteristics were monitored (Figure 11). The device fabricated with a TFB(50 nm)/ F8BT(50 nm) bilayer was added for the pulse measurements in order to address the important role of different-length scale polymer−polymer interfaces in the charge-carrier transport and recombination processes. The pulsed measurements revealed a remarkably clear trend through the appearance of a "turn-on" spike in the EL output of the devices. This "turn-on" spike was strongest in the bilayer device and gradually decreases as the length scale of the organic interfaces decreases, starting with micron scale in the blend and ending with molecular scale in the RC. Therefore, no turn-on spike was observed in the RC. The turn-on spikes were not observed either in the neat F8BT or neat TFB devices.

This turn-on spike can be understood by associating it with charge balance inside the active layer after an initial electrical excitation, although its exact origin has not yet been clearly established.[45] An ohmic contact is formed at the cathode interface between F8BT and Ca electrode since the F8BT energy level for electron injection (i.e., LUMO level, ~2.95 eV) lies very closely to the work function of Ca electrode (~2.9 eV). Hence once a contact is made, there is no injection barrier for

(45) Pinner, D. J. Ph.D. thesis, University of Cambridge (2000).
(46) Tessler, N. *Adv. Mater.* **1999**, *11*, 363.

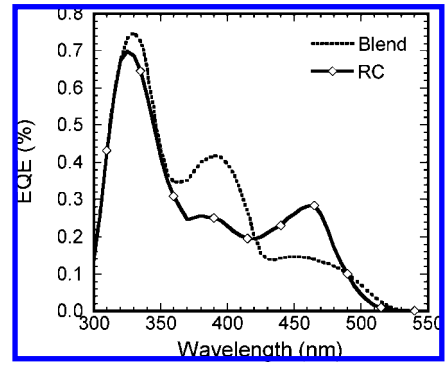

Figure 12. External quantum efficiency (EQE) as a function of excitation wavelength for the blend and RC photovoltaic devices fabricated with ITO/ PEDT:PSS anode and Al cathode.

electrons, and this provides a barrier-free injection of electrons into the F8BT layer even before the driving voltage is applied. Inside the bilayer device, this would lead to an accumulation of electrons at the interface between TFB and F8BT layers due to the energy barrier for electrons induced by the relatively low LUMO level of TFB (~2.25 eV). When a voltage pulse is applied, holes are injected into the TFB layer and meet the high density of electrons already accumulated at the TFB/F8BT interface to recombine and give rise to light emission; thus, a sudden spike can appear in the EL. As time passes, the accumulated electrons quickly run out and the flow of opposite charges becomes more balanced and thus produces more constant EL.

In the blend device, micrometer-length scale TFB-rich phases are dispersed in a F8BT-rich matrix. This F8BT-rich matrix may provide a reasonable pathway for the electron injection and transport, leading to accumulation of barrier-free injected electrons upon contact with Ca cathode. Once the voltage pulse is applied, the flow of holes into the active layer would cause a similar but smaller turn-on spike as that seen in the bilayer. The smaller turn-on spike in the blend device can be understood since freely injected electrons are distributed more evenly throughout the whole active layer, differently from the bilayer device in which high density accumulation of electrons occurs at the abrupt TFB/F8BT interface. As the length scale of the TFB/F8BT interfaces decreases in the copolymer, no accumulation of electrons is expected. In the RC device, where no continuous pathway for the electron transport is present because of randomly distributed TFB and F8BT interfaces at a molecular scale, no turn-on spike is observed. Note that the absence of the turn-on spike in the RC does not depend on the voltage applied (Figure 11b). This observation agrees well with the single-carrier device data, confirming a better charge balance in the RC which produces more stable characteristics of LEDs in terms of device efficiencies.

c. Photovoltaic Devices. Charge photogeneration properties of the materials were studied by characterizing their photovoltaic devices. The external quantum efficiency (EQE) as a function of excitation wavelength is shown for the blend and RC devices (Figure 12). In general, the short-circuit photocurrent action spectra for the blend and RC devices follow the absorption spectra of the active layers, showing the three distinguishable photocurrent peaks at 460, 390, and 320 nm where the absorption peaks of each F8BT and TFB homopolymer appear (Figure 4). The EQE at 460 nm, where the electronic transition

Table 1. Summary of Experimental Results

techniques	blend	RC
DSC	crystallization and melting transitions in F8BT	no crystallization and melting transitions
AFM/optical microscopy	micrometer-length scale lateral-phase separation, rough surface	no lateral-phase separation, smooth surface
Raman	TFB-rich domains surrounded by F8BT-rich matrix	uniformly distributed TFB (∼55 ± 5%) and F8BT (∼45 ± 5%) components
UV−vis absorption	linear combination of TFB and F8BT	blue-shift in the lowest absorption band
PL spectra/decay time	combination of TFB (0.7 ns) and F8BT (2.0 ns) emissions in dilute solution	red-shifted and longer-lived (2.6 ns) F8BT emission with very little TFB emission in dilute solution
Transient PL spectra	efficient interchain energy transfer from TFB to F8BT, TFB decays within ∼10 ps	much faster energy transfer from TFB to F8BT, TFB decays within ∼1 ps
PL efficiencies	0.6−0.65	0.4−0.45
PIA	50% increase in triplet absorption	7.5 times increase in triplet absorption
single-carrier devices	lower hole current than TFB, a large difference between hole and electron currents	lower electron current than F8BT, more balance between hole and electron currents at high voltages
LEDs	high initial efficiencies (10 lm/W, 8 Cd/A) with fast decay at high current	low initial efficiencies (3 lm/W, 3 Cd/A), but much slower decay at high current
transient EL	turn-on spike	no turn-on spike
PVs	higher EQE at the absorption bands at short wavelengths	two times higher EQE at the lowest absorption band

involves a charge transfer state of F8BT,[47,48] is two times higher in the RC than in the blend (0.3% vs 0.15%) but becomes lower at shorter excitation wavelengths (0.25% vs 0.4% at 390 nm and 0.7% vs 0.75% at 320 nm) where the transitions to more delocalized π orbitals of the TFB and F8BT polymers occur.[40,47] We notice that the EQE values measured from the RC device are much lower than those expected from its significantly low PL quantum yield compared to the blend (0.4−0.45 vs 0.6−0.65). This suggests that rather than the formation of free charges under photoexcitaion, other loss mechanisms such as the formation of nonradiative triplet excitons and weakly emissive exciplex states contribute more significantly to the reduction of the PL quantum yield in the RC. This is expected since bound triplet excitons and exciplexes are not likely to be dissociated into free charges to enhance the photocurrent.

The experimental results are summarized in Table 1, and they show significant changes in optoelectronic and charge transport properties of F8BT:TFB interfaces, when two dissimilar conjugated polymers are blended together to form interchain interfaces (blend) or when they are covalently attached to the conjugated backbone to form intrachain interfaces (copolymer).

Quantum-Chemical Calculations. Quantum-chemical calculations have been performed based on semiempirical approaches to understand the electronic structure and associated optical and charge-transport properties of the materials studied here. The ground-state geometry of the representative oligomers of TFB, F8BT, and RC was first optimized at the semiempirical Hartree−Fock Austin Model 1 (AM 1) level[49] in the gas phase (In the calculations, the alkyl side chains attached to the conjugated backbone were replaced by hydrogen atoms). It has been previously shown that the lowest energy conformation of the TFB molecule in the ground state is characterized by a torsion angle of ∼40° between adjacent f8 and phenylene units and by a torsion angle of ∼35° in the tfb moiety (between the plane defined by one of the benzene rings and the plane defined by the central nitrogen atom and the three connected carbon atoms).[40] For the F8BT molecule, the conjugated planes of the f8 and bt units are twisted with respect to one another by ∼47°. These conformations found in TFB and F8BT molecules are preserved in the RC chain, in which the tfb unit in TFB and the bt unit in F8BT are covalently attached to the f8 backbone.

On the basis of their optimized geometries, the electronic structure of the molecules was calculated by using the spectroscopic version of the semiempirical Hartree−Fock intermediate neglect of differential overlap (INDO) method.[48,50] Figure 13 displays the one-electron energy diagram of the TFB, F8BT, and RC monomers, showing how the frontier electronic levels of the f8 chains are affected by the incorporation of both tfb and bt units. In TFB, the HOMO is located mainly on the tfb unit and spreads slightly to the f8 unit, and the LUMO is delocalized along the conjugated backbone; in contrast, in F8BT, the LUMO is strongly localized on the bt unit and the HOMO is delocalized along the conjugated backbone.

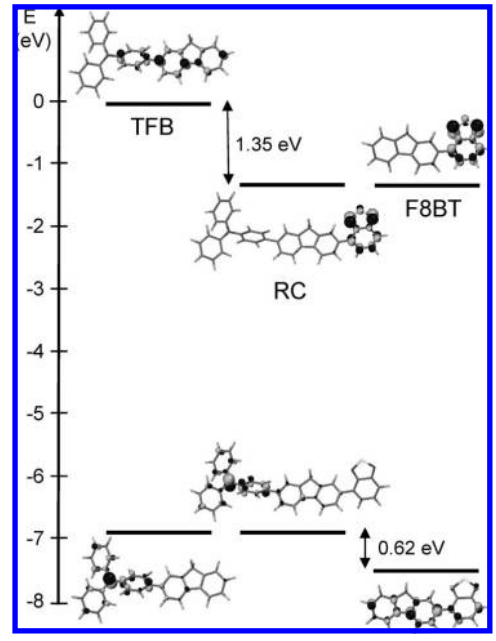

Figure 13. Energies and shapes of the HOMO and LUMO orbitals calculated at the INDO level; the size and color of the circles describe the amplitude and sign of the LCAO (linear combination of atomic orbitals) coefficients associated with the atomic π-orbitals.

(47) Jespersen, K. G.; Beeneken, W. J. D.; Zaushitsyn, Y.; Yartsev, A.; Andersson, M.; Pullerits, T.; Sundstrom, V. *J. Chem. Phys.* **2004**, *121*, 12613.
(48) Cornil, J.; Gueli, I.; Dkhissi, A.; Sancho-Garcia, J. C.; Hennebicq, E.; Calbert, J. P.; Lemaur, V.; Beljonne, D.; Bredas, J. L. *J. Chem. Phys.* **2003**, *118*, 6615.
(49) Dewar, M. J. S.; Zoebisch, E. G.; Healy, E. F.; Stewart, J. J. P. *J. Am. Chem. Soc.* **1985**, *107*, 3902.

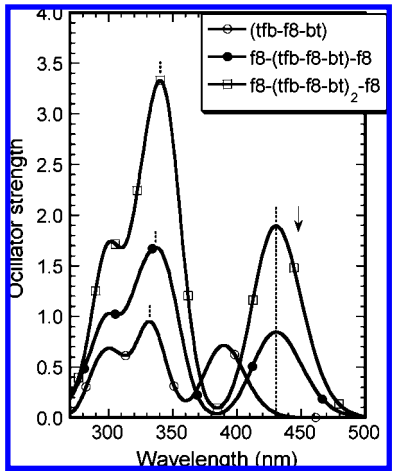

Figure 14. Absorption spectra of the RC molecules calculated at the INDO/SCI level, in which the absorption features are broadened by Gaussian functions with fwhm of 0.3 eV. An arrow at 488 nm indicates the calculated lowest absorption peak position of F8BT oligomer.

This localization scheme for the frontier electronic levels found in the TFB and F8BT molecules is also observed in the RC; i.e. the HOMO lies mainly on the tfb unit and spreads to the conjugated f8 backbone, and the LUMO is strongly localized on the bt unit as in F8BT. This can be rationalized on the basis of the large energy separation (~1.35 eV) between the LUMO levels of TFB and F8BT which reduces the amount of mixing between them. On the other hand, the smaller energy separation (~0.62 eV) between the corresponding HOMO levels is expected to promote further delocalization between the building blocks.

The absorption spectra of all the molecules were also simulated by combining the INDO method to a single configuration interaction (SCI) scheme.[40,48] All of the singly excited configurations created by promoting a single electron from one of the π-occupied levels to one of the π-unoccupied levels are included in the CI expansion to ensure size-consistency.[40,48] The absorption spectrum of the F8BT oligomer containing five f8 units and four bt units has been previously calculated and found to display two main absorption peaks: the lowest peak calculated at 448 nm (2.77 eV) arises from the $S_0 \rightarrow S_1$ excitation involving a charge-transfer transition from the f8 to the bt unit; the second peak at 298 nm (4.16 eV) is due to the $S_0 \rightarrow S_9$ transition involving delocalized π orbitals.[47] In the TFB oligomer, the calculated lowest optical transition appears at a much higher energy (~3.5 eV) due to the increased HOMO−LUMO energy gap.[49]

Here, the absorption spectra of the RC molecules was simulated as a function of chain length, starting with a monomeric RC unit [tfb-f8-bt], adding an f8 unit to each end of the monomer [f8-(tfb-f8-bt)-f8] and increasing the chain-length to form a dimeric RC unit [f8-(tfb-f8-bt)$_2$-f8] (Figure 14). By doing so, the effects of hole-transporting tfb and electron-transporting bt units and f8 bridges on the position and strength of the electronic transitions and their dependence on the length of RC chain were investigated. The absorption spectrum of RC is in general a combination of the absorption spectra of TFB and F8BT and exhibits three main peaks at 390 nm (3.18 eV), 331 nm (3.72 eV), and 300 nm (4.13 eV). The lowest optical transition peaks at 390 nm (3.18 eV) for the (tfb-f8-bt) molecule and shifts to 431 nm (2.88 eV) by adding the f8 units to the end of the monomer [f8-(tfb-f8-bt)-f8]. This absorption peak, however, does not shift any further toward longer wavelengths in a longer RC chain. The second optical transition that appears at 331 nm (3.72 eV) shifts gradually toward a longer wavelength, i.e. to 336 nm for [f8-(tfb-f8-bt)-f8] and 341 nm for [f8-(tfb-f8-bt)$_2$-f8] as the length of the RC chain increases. This effect originates from the different nature of the singlet excited states associated with these transitions in the RC. While the lowest excited state (at 431 nm) is confined on a pair of neighboring bt and f8 units, the higher-lying excited state (at 331 nm) is more delocalized over the whole chain.

We notice that the lowest optical transition in the RC oligomer is blue-shifted by ~0.11 eV with respect to that in the F8BT oligomer. This is in good agreement with the experimental value of ~0.1 eV obtained from the absorption spectra of F8BT and RC dilute solutions (Figure 5). This result clearly corroborates our hypotheses that the tfb unit acts to reduce the conjugation along the polymer chain when incorporated into the rigid conjugated backbone of F8BT.

Together with the measured absorption and emission spectra in RC, we conclude that the bulky and twisted hole-transporting tfb units incorporated at a molecular level into the rigid F8BT polymer backbone have two main electronic effects. First, in the ground-state geometry (absorption), it reduces the effective conjugation length of the F8BT polymer and gives rise to a blue-shift in the absorption spectrum. Second, in the excited-state geometry (emission), it contributes to the formation of a singlet exciton with an enhanced charge-transfer (CT) character and results in a red-shift.

Note that the formation of an intrachain excited state with a strong CT character is relatively easy in the copolymer. This is because the frontier electronic levels in the copolymer are delocalized asymmetrically over the donor and acceptor units of the polymer backbone, so it is easy when linking these donor and acceptor units covalently to form the intramolecular CT state. Compared to the intrachain CT state in the copolymer (covalently linked), the formation of an interchain CT state in the blend (with van der Waal-type interactions) is not so easy. The nature of the excited state (i.e., the degree of CT character) in the blend will depend strongly on the actual packing of the two chain segments.[51] Therefore, it will be extremely difficult to control the packing of these different chain segments to generate a species like the intrachain one.

Such an intrachain CT state has been observed in other conjugated donor−acceptor molecules and polymers containing electron-donating carbazole and phenothiazine units and the electron-accepting phenylquinoline unit for example.[19] A large positive solvatochromism was also observed in the absorption and emission spectra of its oligomers in solutions and films due to a strong intramolecular CT character between the donor and acceptor moieties.[19] An experimental and theoretical investigation of such a solvatochromic effect in RC is in progress, focusing on the absorption and emission spectral changes associated with its geometric relaxation as the solvent polarity is changed.

Conclusions

We have studied optoelectronic and charge-transport properties at organic−organic semiconductor interfaces formed in-

(50) (a) Zerner, M. C.; Loew, G. H.; Kichner, R.; Mueller-Westerhoff, U. T. *J. Am. Chem. Soc.* **1980**, *102*, 589. (b) Zerner, M. C.; Loew, G. H.; Kichner, R.; Mueller-Westerhoff, U. T. *J. Am. Chem. Soc.* **2000**, *122*, 3015.
(51) Huang, Y.-S.; Westenhoff, S.; Avilov, I.; Sreearunothai, P.; Hodgkiss, J.; Deleener, C.; Friend, R. H.; Beljonne, D. *Nat. Mater.* **2008**, *7*, 483.

tramolecularly by a random copolymerization of TFB (electron-donor) and F8BT (electron-acceptor) polymers. These properties were compared to those obtained from TFB:F8BT blend systems which produce organic−organic interchain interfaces at micron-length scale. Our results show that an incorporation of a bulky and twisted triarylamine unit into a rigid F8BT conjugated backbone leads to significant changes in optical and electronic properties of F8BT. For example, the triarylamine unit reduces a conjugation of the F8BT, giving rise to a blue-shift in its absorption spectrum, but it assists the formation of an excited state which has a strong charge-transfer character. This induces a decrease in the optical energy gap of the polymer, leading to a more red-shifted and longer-lived emission than that of F8BT. Compared to the blends, the extremely efficient and much faster energy transfer from tfb donor to bt acceptor was observed in the RC. This efficient energy transfer in the RC was found to be associated with its low PL efficiency due to the migration of radiative singlet excitons to low-energy states such as triplets and exciplexes that are nonemissive or weakly emissive. On the other hand, the presence of molecular-scale tfb-f8-bt interfaces in the RC does not strongly hinder an efficient transport of charge carriers at high drive voltages. Instead, the RC provides a better balance of charge carriers inside the device, which leads to slower decay of the device efficiencies with increasing the drive voltage and thus more stable LEDs than the blend devices. These observations have important implications for fabricating efficient electronic devices using conjugated polymers as an active material, since the performance of these devices will strongly depend on optoelectronic and charge transport properties of electroluminescent conjugated polymers and their interfaces.

Acknowledgment. The authors thank CDT for the materials, Dr. I. Grizzi for valuable comments, D. Lindsey for photothermal deflection spectroscopy (PDS) measurements, and the EPSRC for an Advanced Research Fellowship (J.S.K.). D.B. and J.C. are FNRS research fellows.

JA803766J